Absolute integrated cross sections for some O_2 Herzberg I transitions near 248–249 nm

Zhen-Chuan Bao
Department of Atmospheric, Oceanic, and Space Sciences, University of Michigan, Ann Arbor, Michigan 48109-2143

Wa On Yu
Department of Chemistry, University of Michigan, Ann Arbor, Michigan 48109-1055

John R. Barker[a)]
Department of Atmospheric, Oceanic, and Space Sciences and Department of Chemistry, University of Michigan, Ann Arbor, Michigan 48109-2143

(Received 20 December 1994; accepted 27 March 1995)

A frequency doubled tunable dye laser system with $\sim$0.4 cm^{-1} resolution was used to measure the integrated absorption cross sections of more than 20 rotational transitions in the O_2 Herzberg I ($A\ ^3\Sigma_u^+ \leftarrow X\ ^3\Sigma_g^-$) 8-0 and 9-0 vibrational bands near 248 nm and 249 nm. Oxygen pressures from 200 to 800 Torr and path lengths from 5 to 25 m were employed. The measured absorbances were fitted using a nonlinear least squares analysis and Beer's Law to obtain absolute values for the individual transition integrated cross sections in good agreement with a recent spectral simulation and experimental data. By using the spectral simulation in conjunction with the present experimental results, total oscillator strengths in reasonable agreement with literature values were estimated for the 8-0 and 9-0 vibrational bands. © *1995 American Institute of Physics.*

I. INTRODUCTION

Recently, it was found that the laser irradiation of pure O_2 at 248 nm produces ozone, even though the threshold wavelength for dissociation of O_2 is near 242 nm.[1–3] The studies showed that the O_3 formation involves two processes; initiation, which ''seeds'' the system with O_3, and autocatalysis, which accelerates the O_3 growth. Once ozone is present, the autocatalysis appears to be due to the photolytic production of vibrationally excited O_2 ($X\ ^3\Sigma_g^-$), which subsequently absorbs a second photon during the same laser pulse and dissociates to produce still more ozone by reaction with O_2. The initiation process is less well-characterized, but Shi and Barker[3] found that it is independent of temperature and conjectured that the O_2 $A\ ^3\Sigma_u^+$, $A'\ ^3\Delta_u$, and $c\ ^1\Sigma_u^-$ states (which are generated by absorption near 248 nm) may be involved in reactions with ground state O_2 ($X\ ^3\Sigma_g^-$) to produce ozone and oxygen atoms,

$$O_2(A\ ^3\Sigma_u^+,\ A'\ ^3\Delta_u,\ \text{or}\ c\ ^1\Sigma_u^-) + O_2(X\ ^3\Sigma_g^-) \rightarrow O(^3P) + O_3(X\ ^1A_1). \quad (1)$$

For O_2 energized with a 248 nm photon, such reactions are exothermic and may have low activation barriers, thus explaining the lack of temperature dependence. Very recently, Copeland and co-workers produced specific vibrational and rotational states of O_2 ($A\ ^3\Sigma_u^+$) with one tunable laser and then detected oxygen atoms by laser induced fluorescence,[4] essentially confirming the conjecture by Shi and Barker.

Reaction (1) may help to account for the 10%–50% discrepancies between model calculations (based on satellite measurements of trace species concentrations) of atmospheric odd oxygen ($O_x = O + O_3$) and the observed abundances. Typically, the observed O_x exceeds the calculated concentrations and the discrepancies are greater at higher altitudes.[5–10] The most important source of atmospheric O_x is photodissociation of O_2. Shi and Barker[3] calculated that reaction (1) can contribute an additional 5%–10% O_x and the maximum estimated contribution occurs near the stratopause.

The Herzberg I system of O_2 is the strongest of the three forbidden transitions near 248 nm in O_2; Herzberg I ($A\ ^3\Sigma_u^+ \leftarrow X\ ^3\Sigma_g^-$), Herzberg II ($c\ ^1\Sigma_u^- \leftarrow X\ ^3\Sigma_g^-$), and Herzberg III ($A'\ ^3\Delta_u \leftarrow X\ ^3\Sigma_g^-$). The $A\ ^3\Sigma_u^+$, $A'\ ^3\Delta_u$, and $c\ ^1\Sigma_u^-$ states of O_2 are sometimes designated the ''Herzberg states'' (because they were investigated by Herzberg[11]) or the ''*ungerade* states'' and they are produced in the atmosphere by absorption of sunlight and in the O-atom recombination reaction to form O_2. The Herzberg states and their possible involvement in reactions similar to Reaction (1) have a venerable history, as described by Slanger.[12] Absorption in the Herzberg I continuum ($\lambda < 242$ nm) is the main source of odd oxygen below 80 km and the Herzberg I band system ($\lambda > 242$ nm) is an important contributor to the ultraviolet night airglow.[13,14]

The motivation for the present work is to determine the absolute concentrations of O_2 ($A\ ^3\Sigma_u^+$) produced by irradiation with a 248 nm KrF excimer laser. By comparing the absolute production of O-atoms to the absolute concentration of O_2 ($A\ ^3\Sigma_u^+$) produced by the laser, the efficiency of Reaction (1) in competition with other processes, including the reportedly efficient energy transfer to produce O_2 ($b\ ^1\Sigma_g^+$),[15] can be determined. Since the excimer laser emission band is 50–100 cm^{-1} wide and the O_2 absorption is confined to narrow lines with small cross sections, the O_2 absorbs very little of the laser light and direct absorption measurements using the 248 nm laser are not useful. A frequency doubled tunable

a)Address correspondence to this author.

 0021-9606/95/103(1)/6/8/$6.00

dye laser has sufficient resolution to carry out the measurements, however.

The absorption cross section of O_2 in this wavelength region has been studied by several investigators, but most did not use photoelectric techniques or they used insufficient resolution to resolve rotational transitions. Ditchburn and Young[16] used a photographic technique to determine the absorption cross sections between 185 and 250 nm. Shardanand[17] employed a more accurate photoelectric technique to measure the total absorption of radiation in the 200–280 nm region for both O_2 and the O_2 dimer (O_4) and extrapolated the absorption cross section to zero pressure in order to identify and eliminate contributions due to the dimer. Neither of these investigations resolved rotational structure in the band system. Hasson *et al.*[18] derived a table of absolute band strengths by scaling the relative measurement of Degen and Nicholls[19] to an absolute measurement of the (7,0) band. Hasson and Nicholls[20] then employed a photographic method to determine absolute absorption cross sections for eight vibrational bands ($v''=0$, $v'=4-11$) of the Herzberg I system. These measurements detected some rotational structure, but the accuracy of the results was limited, due to the use of photographic rather than photoelectric detection. In 1989, Bates[21] calculated the transition probabilities for several bands ($v''=0$, $v'=0-11$) of the Herzberg I system, based on the *ab initio* transition moment computations of Klotz and Peyerimhoff,[22] but the values he obtained are larger than the best experimental values. Recently, Huestis *et al.*[23] used cavity ring-down spectroscopy (CRDS) to investigate the O_2 spectrum between 243 and 258 nm and determine the oscillator strengths for all three Herzberg systems. These authors evaluated the literature experimental data along with their own experimental results and proposed ''recommended'' values for the oscillator strengths associated with each band. While the present manuscript was in preparation, we learned of new Fourier transform spectroscopy (FTS) measurements of the Herzberg I transition integrated cross sections carried out by Yoshino and co-workers.[24]

In this paper, we report direct absorption measurements of more than 20 rovibronic bands in the Herzberg I system. We used a direct Beer's law absorption method, which is very simple in concept. The data were analyzed by a least-squares technique and a propagation of errors analysis was carried out to assess the magnitude of the statistical uncertainties. For comparison with the band oscillator strengths reported in other work, we used our results in conjunction with estimates[25] of the contributions made by individual rotational transitions, according to the DIATOM spectral simulation computer code.[23] Calculated in this way, our results for the Herzberg I ($A\ ^3\Sigma_u^+ \leftarrow X\ ^3\Sigma_g^-$) 8-0 and 9-0 band oscillator strengths are in reasonable agreement with the oscillator strengths ''recommended'' by Huestis *et al.*[23]

II. EXPERIMENT

The experimental apparatus is shown schematically in Fig. 1. The equipment consists of a dye laser (Lumonics HyperDye-300) pumped by a XeCl (308 nm) excimer laser (Lumonics HyperEx-400), a second harmonic generating

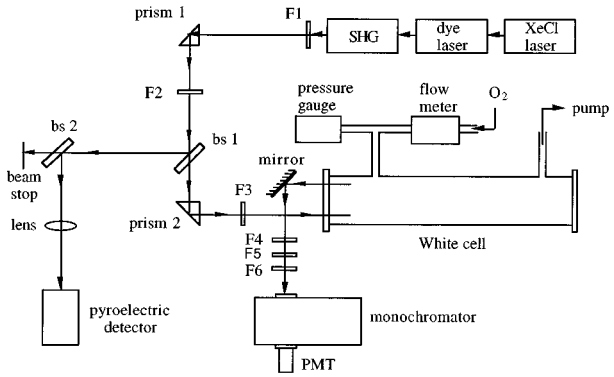

FIG. 1. Experimental apparatus. F1–F6 are color glass filters, bs 1 and bs 2 are beam splitters.

(SHG) unit equipped with a BBO crystal (INRAD AutoTracker-II), a multipass White cell[26] with a distance of 123.0 cm between the end mirrors, a monochromator (Jarrell-Ash Model NO3) and a photomultiplier (Hamamatsu 1P28), and a pyroelectric detector (Molectron Model P3-01). A Scientech volume absorbing calorimeter power meter was also used to monitor absolute laser fluence.

Pulsed laser light in the 248–249 nm wavelength region was produced using Coumarin 498 dye and frequency doubling. The dye laser was scanned at a rate of 0.02 cm^{-1}/s with a maximum scan range of 15 cm^{-1}. The pulsed (30 Hz) output from the SHG had a typical linewidth of $\sim$0.4 cm^{-1} with energy $\approx$0.6 mJ per pulse.

A dual-beam arrangement was used in order to correct for laser power fluctuations. The UV laser light was split into two paths by the uncoated Suprasil beam splitter #1; one beam (detected by the pyroelectric detector) monitored laser intensity I_L; the other beam passed through the White cell and was detected by the photomultiplier tube (PMT). The monochromator isolated the pulsed ultraviolet light and was used with wide slits in order to transmit all light in the experimental wavelength region investigated in a single scan ($\leqslant$15 cm^{-1}). The intensities of the two light beams were recorded simultaneously in order to account for laser power fluctuations. Six color glass filters (F1–F6) were used as shown in Fig. 1 to eliminate visible laser light and reduce the ultraviolet light intensity to within the linear range of the detectors. The linearity of the detection system was verified by inserting several colored glass filters with known optical depth into the light path and monitoring the intensity of the output signals. The signals were amplified (Tektronix AM502) and sent to two channels of a boxcar signal averager (SRS SR250). The boxcar gate was set near the peak output voltage for each channel ($\sim$15 μs) and continuous averaging (typically 100 shots) was used. Two digital oscilloscopes (LeCroy 9400) monitored the signals. As the dye laser was scanned, the two averaged signals and a ramp voltage proportional to wavelength (from the dye laser scan-controller) were recorded simultaneously using LabView-2 software installed on a Macintosh computer. The data were preserved as computer files and processed later.

Because of the very small absorption cross section of the Herzberg I bands, the measurements required high pressure

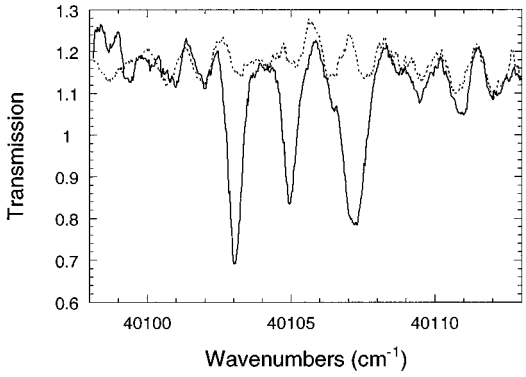

FIG. 2. Comparison of I (transmittance with O_2 in cell, solid line) and I_0 (transmittance with no O_2 in cell, dashed line). Experimental conditions, 800 Torr O_2, path length 1968 cm.

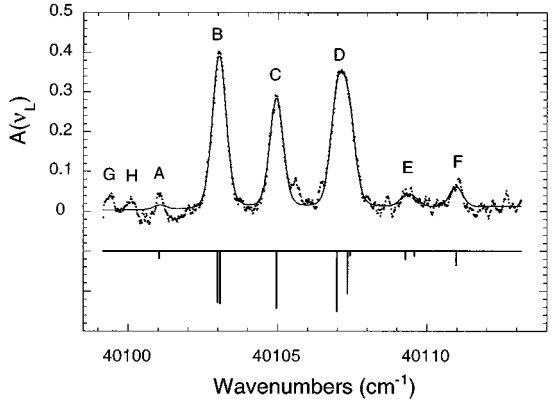

FIG. 3. O_2 Herzberg I (8,0) band near 249 nm for the data shown in Fig. 2. The inverted stick figure shows the expected (Ref. 25) positions and relative intensities of individual transitions.

and/or long optical path length of the O_2. We employed a 123.0 cm White cell with aluminum-coated mirrors adjusted for 4–20 passes to produce a total path length of 492–2460 cm. The cell consisted of a Pyrex glass cylindrical pipe ~8 cm in diameter equipped with aluminum end-plates vacuum sealed to the Pyrex cell with silicone high vacuum grease. The front end-plate had two quartz windows for incoming and exiting light. We utilized a flowing system for our measurements in order to minimize O_3 accumulation and we employed an electronic mass flow meter (MKS model 500-SCCM) to control the flow rate, which was maintained at 500 sccm. The cell was equipped with a capacitance manometer (MKS Baratron 0–1000 Torr) and experiments were carried out with pressures ranging from 200 to 800 Torr of O_2. For conversion of pressures to concentrations, the average temperature was assumed to be 298 K. In all experiments, ultrahigh purity (99.993%) O_2 was used as delivered from the manufacturer (Liquid Carbonic Specialty Gas Corporation). We estimate that the average uncertainty in pressure and path length was about 2%.

Because the optical components and mirrors in the optical train and White Cell may introduce minor absorbances and since the O_2 absorbance is very low, it is necessary to account for the optical transmission of the system in the absence of O_2. It is also necessary to account for laser intensity (I_L) fluctuations. This was accomplished by using a dual beam arrangement and monitoring the light intensity of both beams during two separate scans of the laser frequency ν_L. In scan (a), the intensity (I_0) of the light transmitted through the empty cell was recorded, along with the laser intensity (I_L). In scan (b), O_2 was present in the cell when the laser intensity and transmitted light intensity (I) were measured. The results of the two scans were then combined to obtain the absorbance due to the O_2,

$$A(\nu_L)=1-\frac{[I(\nu_L)/I_L(\nu_L)]_b}{[I_0(\nu_L)/I_L(\nu_L)]_a}. \tag{2}$$

In this way, corrections are applied for laser power fluctuations and for possible absorptions in the optical system which are not due to O_2. Figure 2 shows $[I_0(\nu_L)/I_L(\nu_L)]_a$ and $[I(\nu_L)/I_L(\nu_L)]_b$ for one of the groups of transitions in the Herzberg I (8,0) band system with 16 passes and 800 Torr of O_2; the absorbance derived from the same data are shown in Fig. 3. These results are in good quantitative agreement with absorption data obtained by Slanger *et al.*,[27] as discussed below.

III. RESULTS AND DISCUSSION

The absorption cross section can be obtained by fitting the experimental data by nonlinear least squares. The laser intensity, the transmitted intensity in the absence of O_2, and that in the presence of O_2 (I_L, I_0, and I, respectively) can be written

$$I_L(\nu_L)=\int_0^\infty w(\nu)d\nu, \tag{3}$$

$$I_0(\nu_L)=\int_0^\infty w(\nu)\alpha(\nu)d\nu\approx\alpha(\nu_L)\int_0^\infty w(\nu)d\nu, \tag{4}$$

$$I(\nu_L)=\int_0^\infty w(\nu)\alpha(\nu)e^{-\sigma(\nu,\nu_L)xN}d\nu$$

$$\approx\alpha(\nu_L)\int_0^\infty w(\nu)e^{-\sigma(\nu,\nu_L)xN}d\nu, \tag{5}$$

where $w(\nu)$ is the laser line shape function, $\alpha(\nu)$ is the White cell mirror reflectance function, ν_L is the central laser frequency, N is the absorber concentration, x is the absorption path length, and $\sigma(\nu)$ is the total O_2 absorption cross section. Because $\alpha(\nu)$ is expected to vary slowly with the frequency, it can be treated approximately as a constant over the small range of integration, as shown.

We assumed that the laser line is Gaussian. Thus, $w(\nu)$ was written

$$w(\nu,\nu_L)=w_0(\nu_L)\exp\{-4\ (\ln 2)[(\nu-\nu_L)/w_D]^2\}, \tag{6}$$

where $w_0(\nu_L)$ is the amplitude and w_D is the Doppler full-width at half-maximum of the laser line. Because both Doppler and pressure broadening existed under our experimental conditions, we assumed the O_2 absorption line shape is described by the Voigt profile, which is a convolution of Doppler and Lorentzian profiles. Because the Voigt profile is expressed as an integral which must be carried out numerically,

least-squares analysis would be prohibitively expensive in computer time. Thus, we employed a reasonably accurate closed-form approximation of the Voigt profile which lends itself to rapid calculation and is claimed to be accurate to within 3% or less.[28] For n rotational transitions, the approximate expression is written

$$\sigma(\lambda,\lambda_i)=\sum_{i=1}^{n}\sigma_i(\lambda_i)\left(\left(1-\frac{w_L}{w_V}\right)\exp\left[-2.772\left(\frac{\lambda-\lambda_i+\Delta}{w_V}\right)^2\right]+\frac{w_L/w_V}{1+4[(\lambda-\lambda_i+\Delta)/w_V]^2}+0.016\left(1-\frac{w_L}{w_V}\right)\times\left(\frac{w_L}{w_V}\right)\left\{\exp\left[-0.4\left(\frac{\lambda-\lambda_i+\Delta}{w_V}\right)^{2.25}\right]-\frac{10}{10+[(\lambda-\lambda_i+\Delta)/w_V]^{2.25}}\right\}\right), \tag{7}$$

where $\sigma_i(\lambda_i)$ is the amplitude at the center of the ith absorption line and λ_i is the center wavelength of the line. The parameter Δ is the difference between the nominal dye laser wavelength and the actual wavelength of a particular rotational transition (Δ is assumed to be constant for all of the lines in a given wavelength scan), and w_V and w_L are the Voigt and Lorentzian full widths at half-maximum. The Voigt FWHM (w_V) is given by the following function of the Doppler and Lorentzian widths,

$$w_V=\frac{w_L}{2}+\sqrt{[(w_L/2)^2+w_D^2]}. \tag{8}$$

Equation (7) is expressed as a function of wavelength and it is easily transformed to a function of frequency.

In order to account for a potential ''background absorbance'' which could be due to O_2 dimers or other sources, we added two terms to the $A(\nu_L)$ expression on the assumption that the background absorbance varied linearly with frequency (with slope k and intercept d) over the 15 cm^{-1} range of a typical spectral scan,

$$A(\nu_L)=1-\frac{[I/I_L]_b}{[I_0/I_L]_a}+d+k\nu_L. \tag{9}$$

By using Eqs. (3)–(8), Eq. (9) can be used for least squares analysis of the O_2 experimental data. For n rotational transitions in a spectral scan, there are $(n+4)$ parameters; δ_L, Δ, k, d, and $\sigma_i(\nu_L)$, $i=1\ldots n$. The ν_i values were taken from results of a DIATOM spectral simulation,[25] since it provided a convenient tabulation in excellent agreement with literature assignments for the transitions. Note that the DIATOM spectral simulation code intensities were not used in the fitting procedure and thus the present results for integrated cross sections are completely independent of the simulations. The least squares analysis was carried out by using a nonlinear least squares fitting code based on the Marquardt algorithm,[29] which generates an error matrix useful for error propagation, or with a commercial software package (KaleidaGraph v.3.0.1, Abelbeck Software, 1993) for Macintosh computers. The integrated absorption cross section was calculated by using Simpson's rule to numerically integrate Eq. (7) using the fitted Voigt parameters; the integration step size was chosen so that the numerical integrals converged to within 1%.

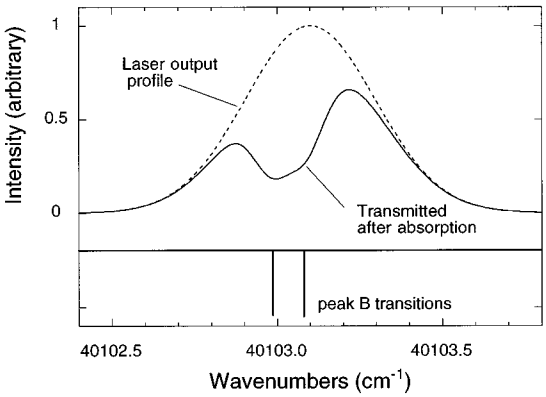

FIG. 4. Simulation showing the laser emission line and the absorption due to peak B. The parameters were obtained by least squares fits of the data presented in Figs. 2 and 3; $\nu_L=40\ 103.1\ cm^{-1}$, $w_L=0.0897\ cm^{-1}$, and $w_D=0.088\ cm^{-1}$.

For all the least squares fits, we assumed that the O_2 absorption line was Doppler and pressure broadened with a calculated Doppler width of $w_D=0.088\ cm^{-1}$ ($T=298$ K). Pressure broadening is due to ''optical collisions'' which effectively shorten the lifetime of the excited state and the parameters depend on rotational state and the nature of the collider gas. Recent Raman spectroscopic measurements of O_2 self-broadening coefficients by Millot *et al.*[30] indicate that the pressure broadening width changes from $\sim$0.02 to $\sim$0.09 cm^{-1} over our experimental pressure range for the transitions investigated. In the least squares fitting procedure, we used the pressure broadening coefficients tabulated in Table I, which are matched to the rotational transitions. The integrated cross section results are not very sensitive to the assumed coefficients; when the pressure broadening coefficients were varied by $\pm$50%, the resulting integrated cross sections varied by only about $\pm$10%. Because the quoted 2σ uncertainties in the O_2 self-broadening coefficients are only $\sim$2%,[30] the effects of errors in the coefficients on our derived integrated cross sections are negligible.

The experimental absorption spectrum derived from the data in Fig. 2 is presented in Fig. 3. The rotational transitions in this small part of the 249 nm region are assigned to the Herzberg I(8,0) rovibronic band and we used the DIATOM spectral simulation[23,25] as a guide to the assignment. Figure 4 displays a simulation showing the relative sizes of the fitted laser width and absorptions due to peak B (see Table I) corresponding to the data presented in Figs. 2 and 3. In Fig. 4, the laser linewidth ($\sim$0.4 cm^{-1}) is greater than the assumed Voigt width and the separation between the two transitions which contribute to peak B. The laser linewidth and Voigt widths contribute in all of the spectra to line overlap. For example, only the six peaks labeled A,B,C,D,E, and F were resolved in Fig. 3, although ten transitions are assigned for this region.[25,31] In addition to the Herzberg I transitions in Fig. 3, peak H is due to two O_2 Herzberg III (9,0) transitions and has been omitted from the analysis. No other detectable transitions from either the Herzberg II or Herzberg III bands

TABLE I. Experimental results.

Peak	Integrated cross section[a] (10^{-25} cm^2 cm^{-1})	Herzberg I transition frequencies[b] (vacuum cm^{-1})	Pressure broadening coefficients[c] (HWHM in 10^{-1} cm^{-1} atm^{-1})	Recommended integrated cross section[d] (10^{-25} cm^2 cm^{-1})	Herzberg I transition assignments[e] (v',v''),N,X
A	2.8±2.0(0.42)	40 101.041 0	42.6±0.8	4.93	(8,0),9,$^QQ_2$
B	72.6±2.6(0.92)	40 102.986 5	42.6±0.8	34.08	(8,0),9,$^QR_{23}$
		40 103.080 8		34.83	(8,0),9,$^QP_{21}$
C	42.4±2.3(0.66)	40 104.951 2	42.6±0.8	37.74	(8,0),9,$^QR_{12}$
		40 106.990 9	42.6±0.8	39.73	(8,0),9,$^QQ_1$
D	76.5±2.6(0.76)	40 107.337 3	42.6±0.8	28.05	(8,0),9,$^QP_{32}$
		40 107.427 4	41.7±0.8	2.85	(8,0),11,$^SR_{21}$
E	8.4±2.1(0.48)	40 109.282 8	42.6±0.8	5.24	(8,0),9,$^QQ_3$
		40 109.582 1	45.3±0.8	3.21	(8,0),7,$^OP_{23}$
F	5.9±2.1(0.44)	40 110.977 0	45.3±0.8	9.45	(8,0),7,$^OP_{12}$
I	3.7±2.1(0.45)	40 221.740 8	36.9±0.8	2.53	(9,0),21,$^QQ_2$
J	12.5±2.1(0.51)	40 223.564 4	36.9±0.8	6.89	(9,0),21,$^QR_{23}$
		40 223.898 2		6.96	(9,0),21,$^QP_{21}$
K	6.3±2.1(0.42)	40 226.224 5	36.9±0.8	7.28	(9,0),21,$^QR_{12}$
L	17.2±2.1(0.65)	40 227.709 4	36.9±0.8	6.31	(9,0),21,$^QP_{32}$
		40 228.381 9		12.11	(9,0),21,$^QQ_1$
M	2.3±2.0(0.41)	40 229.533 0	36.9±0.8	0.14	(9,0),21,$^QQ_3$
N	5.0±2.0(0.26)	40 286.558 0	36.1±0.8	3.44	(9,0),19,$^QQ_2$
O	19.6±2.1(0.35)	40 288.400 0	36.1±0.8	10.92	(9,0),19,$^QR_{23}$
		40 288.697 0		11.04	(9,0),19,$^QP_{21}$
P	12.1±2.0(0.28)	40 291.001 8	36.1±0.8	11.60	(9,0),19,$^QR_{12}$
Q	22.4±2.1(0.36)	40 292.577 7	36.1±0.8	9.90	(9,0),19,$^QP_{32}$
		40 293.140 8		17.88	(9,0),19,$^QQ_1$
R	4.6±2.0(0.40)	40 344.905 2	38.0±0.8	4.36	(9,0),17,$^QQ_2$
		40 345.264 7	36.1±0.8	0.47	(9,0),19,$^SR_{32}$
S	28.8±2.2(0.61)	40 346.765 9	38.0±0.8	16.22	(9,0),17,$^QR_{23}$
		40 347.025 6	38.0±0.8	16.42	(9,0),17,$^QP_{21}$
		40 347.403 8	36.1±0.8	0.12	(9,0),19,$^SQ_{31}$
T	11.4±2.1(0.40)	40 349.297 9	38.0±0.8	17.33	(9,0),17,$^QR_{12}$
U	35.1±2.2(0.63)	40 350.991 1	38.0±0.8	14.54	(9,0),17,$^QP_{32}$
		40 351.418 3		24.71	(9,0),17,$^QQ_1$
V	4.4±2.0(0.26)	40 396.827 5	38.8±0.8	5.14	(9,0),15,$^QQ_2$
		40 398.707 6	38.8±0.8	22.51	(9,0),15,$^QR_{23}$
W	41.6±2.2(0.48)	40 398.720 1	38.0±0.8	0.63	(9,0),17,$^SR_{32}$
		40 398.928 9	38.8±0.8	22.82	(9,0),15,$^QP_{21}$
X	22.2±2.1(0.40)	40 400.840 6	38.0±0.8	0.20	(9,0),17,$^SQ_{31}$
		40 401.154 0	38.8±0.8	24.22	(9,0),15,$^QR_{12}$
Y	49.5±2.3(0.61)	40 403.000 5	38.8±0.8	19.87	(9,0),15,$^QP_{32}$
		40 403.255 4	38.8±0.8	31.91	(9,0),15,$^QQ_1$

[a]Uncertainties ($\pm\sigma$) are total estimated uncertainty, as described in the text. Values in parentheses are $\pm\sigma$ statistical uncertainties.
[b]Transition frequencies from the DIATOM spectral simulation (Refs. 23 and 25).
[c]From Millot *et al.* (Ref. 30).
[d]Recommended integrated cross sections from the DIATOM spectral simulation (Refs. 23 and 25).
[e]Spectroscopic notation after Borrell *et al.* (Ref. 31) and Yoshino *et al.* (Ref. 33); v''=lower state, v'=upper state, N=total angular momentum, X=transition type.

have been reported in any of the spectral ranges considered here. Minor peaks (such as peak G) show up in some of the spectra, but their intensities are not reproducible and they may be due to trace impurities.

The Herzberg I (8,0) absorptions near 249 nm were measured with path lengths ranging from 492 to 2460 cm, and pressures ranging from 200 to 800 Torr of O_2. In order to reduce statistical errors, 3 to 9 experimental runs were averaged to obtain each spectrum. We carried out nonlinear least squares fitting to the assigned transitions and used the DIATOM spectral simulation as a guide in determining the important transitions at the temperature of the experiments. The fitted results revealed no significant reproducible "background absorption" and we conclude that O_2 dimer absorption is negligible under our conditions. From the nonlinear least squares fits, we determined the integrated absorption cross sections for peaks A–F individually and collectively (their sum). It is worth noting that all ten peaks assigned for this region were included in the least-squares fitting procedure, but individual components of the overlapping transitions gave highly correlated least squares fits; the individual components are not accurately determined and only the sums of the peak areas are significant in such cases.

Since pressure and path length were both varied, it is

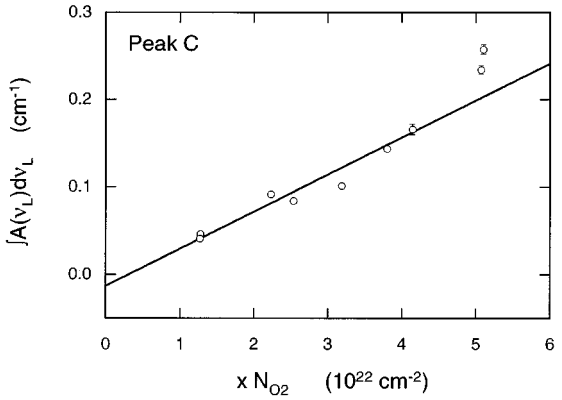

FIG. 5. Integrated absorption coefficient $\int A(\nu_L)d\nu_L$ vs xN_{O_2} for peak C. The solid line is the weighted linear least squares fit.

possible to determine whether the results are consistent with Beer's law. For that purpose, the integrated absorbance $[\int A(\nu_L)d\nu_L]$ determined for peak C (which is due to a single transition) is plotted as a function of the product of O_2 concentration and path length in Fig. 5 (background absorbance was omitted). Similarly, the sum of the integrated absorption coefficients for peaks A–F is presented in Fig. 6. The statistical errors associated with the data presented in Fig. 5 were calculated with propagation of the errors obtained from the error matrix generated by the Marquardt nonlinear least squares algorithm.

The linear least squares fit shown in Fig. 5 was weighted according to the relative errors of the individual experiments. The linear plots in both figures are representative of all of the data and show that the O_2 absorption is consistent with Beer's law under our experimental conditions. The slopes and statistical uncertainties of the fitted lines are the integrated absorption cross sections for peak C and the sum of peaks A–F; $(4.241\pm0.066)\times10^{-24}$ cm and $(2.365\pm0.137)\times10^{-23}$ cm, respectively. The small negative intercepts in both figures have low statistical significance.

These experimental results can be compared with the 249 nm spectrum published by Slanger *et al.*,[27] which covers the wavelength range corresponding to peaks A–D. We extracted the data from their figure and carried out the analysis in exactly the same way as we analyzed our own data. The

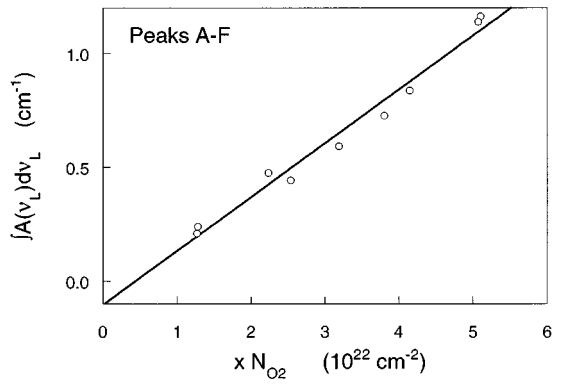

FIG. 6. Integrated absorption coefficient $\int A(\nu_L)d\nu_L$ vs xN_{O_2} for peaks A–F. The solid line is the weighted linear least squares fit.

TABLE II. Integrated absorption cross sections (10^{-25} cm^2 cm^{-1}).

Peak	Slanger *et al.*[a]	Present work[b]	DIATOM spectral simulation[c]
A	4.8	2.8	4.93
B	61.7	72.6	68.91
C	41.4	42.4	37.74
D	64.6	76.5	70.63

[a]Reference 27.
[b]See Table I.
[c]Reference 23.

results are in good agreement, as shown in Table II. There is also good agreement with the FTS measurements carried out on the Herzberg I (8,0) band by Yoshino and co-workers.[24]

For the Herzberg I (9,0) band system (around 248 nm), we measured the spectra of four groups of peaks. All of the spectra were least-squares fitted as outlined above, but the optical path length (16 passes through the White Cell) and O_2 pressure (800 Torr) were not varied. The spectra and least squares fits are shown in Fig. 7. The integrated absorption cross sections derived from the spectra are presented in Table I along with the spectroscopic assignments and transition frequencies of the individual rotational transitions. For comparison, we have listed integrated cross sections obtained from a DIATOM spectral simulation,[25] which is based on the spectroscopic parameters recommended by Huestis *et al.*[23] for the Herzberg I transitions and assuming a temperature of 300 K. The comparison shows good agreement.

We estimate that uncertainties due to pressure and path length average about $\pm2\%$. Uncertainties due to fluctuations in the base line seem to contribute about $\pm2\times10^{-25}$ cm to the integrated cross sections. The base line fluctuations are most apparent in Fig. 7(a), where peak M is of the same order of magnitude as the fluctuations. The total uncertainties tabulated in Table I were estimated assuming that the pressure and path length uncertainties, the base line fluctuation uncertainties, and the statistical uncertainties (from propagation of errors) are independent. Some observed peaks (e.g., peaks M, N, and R) appear to be systematically shifted from the known transition frequencies. In most cases, this shift is due to base line fluctuations, but it is also possible that some nonlinearity is present in some spectral scans. For peak N, the integrated cross section is slightly larger when the peak is refitted by itself using a shifted transition frequency, but the increase is of the same order as the total estimated uncertainty.

The oscillator strength $f(v',v'')$ is related to the integrated band absorption coefficient and the integrated band absorption cross section by the following expression:[20]

$$f=\frac{m_e c^2}{\pi e^2}\int_{\text{band}}\sigma(\nu)d\nu=1.1296\times10^{12}\int_{\text{band}}\sigma(\nu)d\nu, \tag{10}$$

where ν is expressed in cm^{-1}, $\int\sigma(\nu)d\nu$ is the integrated band absorption cross section expressed in cm, m_e and e are the electron mass and charge, respectively, and c is the speed of light. Random errors can be minimized by summing the contributions from all of the transitions observed in the

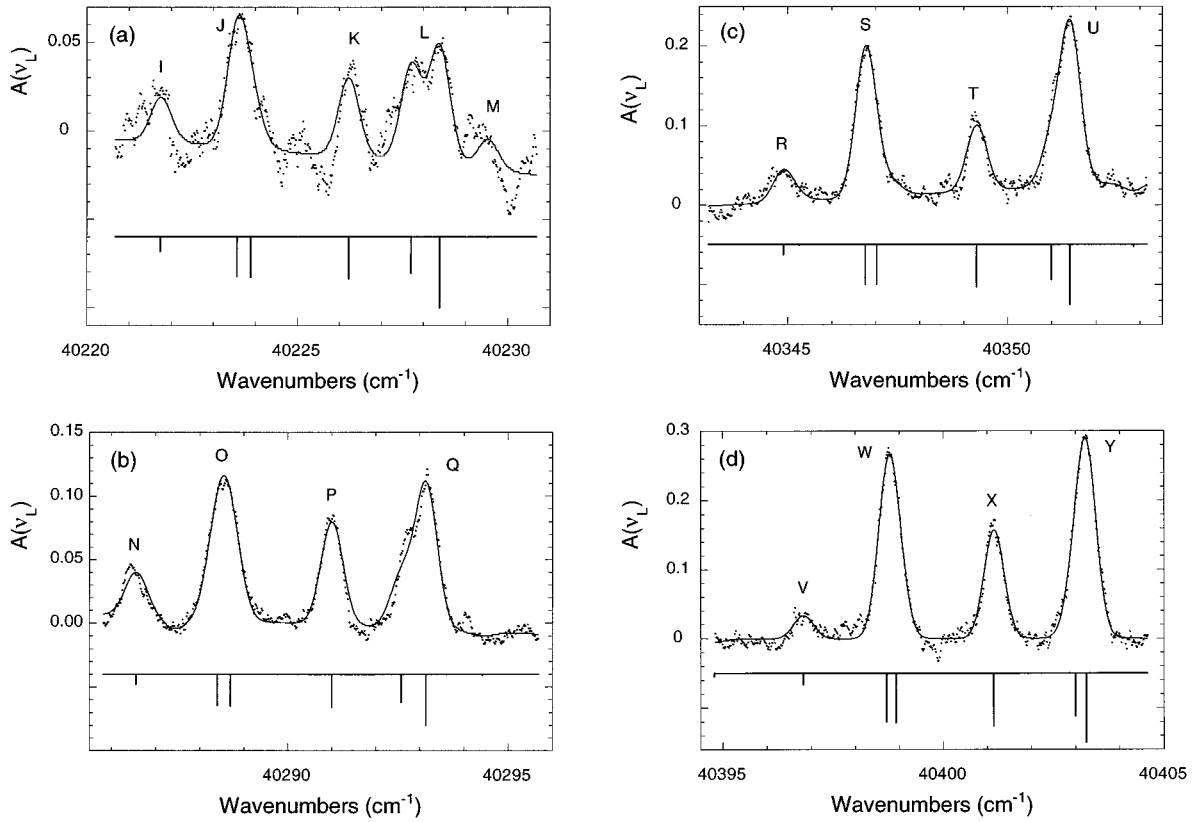

FIG. 7. (a)–(d) Four groups of transitions in the O_2 Herzberg I (9,0) band near 248 nm (800 Torr O_2, path length 1968 cm). The inverted stick figures show the expected (Ref. 25) positions and relative intensities of individual transitions.

present work corresponding to a particular vibrational band. The oscillator strength for the entire band requires integrating $\sigma(\nu)$ over the whole band, but we measured only a few groups of transitions and each group makes only a small contribution to the entire band. Given the relative contribution of each group however, it is possible to use our data to estimate the total oscillator strength for each vibrational band. The relative contribution of each group can be estimated from the DIATOM spectral simulation[23] results provided to us by Huestis[25] for each rotational line in the Herzberg I (8,0) and (9,0) bands at 300 K. From the simulation results, we determined the relative contribution of each group of peaks measured in our experiments and estimated the total band integrated cross sections and oscillator strengths which are presented in Table III along with values from the literature.[23] Note that our integrated cross sections are the result of least-squares fitting and are completely independent of the spectral simulations. Based on our data and the spectral simulation, the estimated oscillator strengths are in reasonable agreement with the other experimental measurements and the recommendations listed in Table III. Because the accuracy of the relative group contributions derived from the spectral simulations is not well known,[23] only statistical errors based on our integrated cross sections are presented in the table.

As mentioned in the Introduction, absorption of sunlight

TABLE III. Herzberg I oscillator strengths (units of 10^{-10}).

Band (v',v'')	Photographic Hasson *et al.*[a]	Revised photographic Hasson and Nicholls[b]	Calculated Bates[c]	Cavity ring down Huestis *et al.*[d]	"Recommended" Huestis *et al.*[d]	Present work[e]
(8,0)	1.63	1.39	2.23	0.88	1.60	1.71±0.05
(9,0)	1.85	1.40	2.64	1.08	1.78	1.66±0.05

[a]Reference 18.
[b]Reference 20.
[c]Reference 21.
[d]Reference 23.
[e]Based on the results in Table I and DIATOM spectral simulations, as described in the text (Ref. 25). Uncertainties ($\pm 1\sigma$) are based only on the integrated cross sections measured in the present work; the spectral simulation uncertainties are not known.

by O_2 ($X\ ^3\Sigma_g^-$) to produce O_2 ($A\ ^3\Sigma_u^+$) can result in odd oxygen production, if O_2 ($A\ ^3\Sigma_u^+$) reacts with O_2 ($X\ ^3\Sigma_g^-$) according to Reaction (1). The present oscillator strength estimates and the other experimental determinations are consistently lower than the calculated values,[21] which were the basis for the odd oxygen production rates estimated by Shi and Barker.[3] If the present results are used, the estimated production of O_2 ($A\ ^3\Sigma_u^+$) must be reduced by about half. The O_x production estimates must be reduced still further, because it was assumed that the only fate of O_2 ($A\ ^3\Sigma_u^+$) is to react according to Reaction (1) and it is now known that this is not its only fate. Bednarek *et al.*[15] recently reported that the quantum yield for physical quenching of O_2 ($A\ ^3\Sigma_u^+$, $v=8$) to produce O_2 ($b\ ^1\Sigma_g^+$, $v=0$) is $\sim$0.25 and Copeland *et al.*[4] have reported that the O-atom quantum yield is less than unity for several vibrational bands in the Herzberg I system. The original estimates for O_x production peaked at about 6% (relative to photodissociation of O_2) near 50 km. Revised estimates would be less than half as large and this source of O_x becomes essentially insignificant. Other explanations[12,32] have been offered for the differences between model calculations and actual observations of O_x abundances. Although molecular oxygen and ozone only contain two and three atoms, respectively, these ''pure oxygen'' chemical systems are very complex, due to the complicated interactions among the many reactive states involved.

ACKNOWLEDGMENTS

We thank T. M. Dunn for the loan of the multipass White Cell. Thanks go to T. G. Slanger and R. A. Copeland for very helpful discussions and copies of manuscripts prior to publication. We thank D. L. Huestis for providing us with the results of his spectral simulations. Thanks also go to K. Yoshino for communicating his unpublished FTS results on the 8-0 band. This work was funded, in part, by NASA (Upper Atmosphere Research Program) and by NSF (Atmospheric Chemistry Division).

[1] T. G. Slanger, L. E. Jusinski, G. Black, and G. E. Gadd, Science **241**, 945 (1988).
[2] J. A. Guthrie, X. Wang, and L. J. Rudziemski, presented at the International Quantum Electronics Conference, 1990 (unpublished).
[3] J. Shi and J. R. Barker, J. Geophys. Res. **97**, 13 039 (1992).
[4] R. A. Copeland, K. Knutsen, and T. G. Slanger, in *Proceedings of the International Conference on Lasers '93* (STS, MacLean, VA, 1994), p. 318.
[5] D. W. Rusch and R. S. Eckman, J. Geophys. Res. **90**, 12 991 (1985).
[6] M. Allen, J. Geophys. Res. **91**, 2844 (1986).
[7] R. T. Clancy, D. W. Rusch, R. J. Thomas, M. Allen, and R. S. Eckman, J. Geophys. Res. **92**, 3067 (1987).
[8] M. B. McElroy and R. J. Salawitch, Science **243**, 763 (1989).
[9] M. Natarajan and L. B. Callis, Geophys. Res. Lett. **16**, 473 (1989).
[10] J. Eluszkiewicz and M. A. Allen, J. Geophys. Res. **98**, 1069 (1993).
[11] G. Herzberg, Can. J. Phys. **30**, 185 (1952).
[12] T. G. Slanger, Science **265**, 1817 (1994).
[13] J. P. Hennes, J. Geophys. Res. **71**, 763 (1966).
[14] D. R. Bates, in *Problems and Progress in Atmospheric Chemistry*, Advanced Series in Physical Chemistry, edited by John R. Barker (World Scientific, Singapore).
[15] G. Bednarek, R. P. Wayne, J. Wildt, and E. H. Fink, Chem. Phys. **185**, 251 (1994).
[16] R. W. Ditchburn and P. A. Young, J. Atmos. Terrest. Phys. **24**, 127 (1962).
[17] Shardanand, Phys. Rev. **186**, 5 (1969).
[18] V. Hasson, R. W. Nicholls, and V. Degen, J. Phys. B Atom. Mol. Phys. **3**, 1192 (1970).
[19] V. Degen and R. W. Nicholls, J. Phys. B **2**, 1240 (1969).
[20] V. Hasson, and R. W. Nicholls, J. Phys. B **4**, 1778 (1971).
[21] D. R. Bates, Planet. Space Sci. **37**, 881 (1989).
[22] R. Klotz and S. D. Peyerimhoff, Mol. Phys. **57**, 573 (1986).
[23] D. L. Huestis, R. A. Copeland, K. Knutsen, T. G. Slanger, R. T. Jongma, M. G. H. Boogaarts, and G. Meijer, Can. J. Phys. **72**, 1109 (1994).
[24] K. Yoshino (private communication, 1994).
[25] D. L. Huestis (private communication, 1994).
[26] J. U. White, J. Opt. Soc. Am. **32**, 285 (1942).
[27] T. G. Slanger, W. K. Bischell, and M. J. Dyer, Chem. Phys. Lett. **108**, 472 (1984).
[28] J. O. Arnold, E. E. Whiting, and G. C. Lyle, J. Quantum Spectrosc. Radiat. Transfer **9**, 775 (1969).
[29] P. R. Bevington, *Data Reduction and Error Analysis for the Physical Sciences* (McGraw–Hill, New York, 1969), p. 237.
[30] G. Millot, R. Saint-Loup, J. Santos, R. Chaux, and H. Berger, J. Chem. Phys. **96**, 961 (1992).
[31] P. M. Borrell, P. Borrell, and D. A. Ramsay, Can. J. Phys. **64**, 721 (1986).
[32] R. L. Miller, A. G. Suits, P. L. Houston, R. Toumi, J. A. Mack, and A. M. Wodtke, Science **265**, 1831 (1994).
[33] K. Yoshino, J. E. Murray, J. R. Esmond, Y. Sun, W. H. Parkinson, A. P. Thorne, R. C. M. Learner, and G. Cox, Can. J. Phys. **72**, 1101 (1994).